INTERPRETATION OF SINGLE-DOPPLER RADAR SIGNATURES IN A V-SHAPED HAILSTORM: PART I – EVOLUTION OF REFLECTIVITY-BASED FEATURES

Rodger A. Brown

NOAA/National Severe Storms Laboratory
Norman, Oklahoma

and

Kathleen L. Torgerson

NOAA/National Weather Service Forecast Office
Pueblo, Colorado

Abstract

Part I of this two-part descriptive study documents the evolution of updrafts, hail, and cloud-to-ground lightning within a North Dakota multicell hailstorm that had a V-shaped radar reflectivity pattern. Details of storm evolution were inferred from single-Doppler velocity and radar reflectivity signatures using a single-Doppler radar analysis technique. Utilizing the analysis technique, new updrafts were deduced to form at the upstream end of the storm at the point of the V shape. After an updraft died, the V shape was maintained as the associated hydrometeors moved down either the right or left storm flank as they descended. The V-shaped storm structure was the result of interactions between individual updrafts and ambient flow.

Evolution of hail within the storm was presumed from the presence of flare echo reflectivity signatures that extended beyond the far side of the storm relative to the radar. When flare echo length was at its greatest, large hailstones the sizes of golf balls to baseballs were reported. The only positive cloud-to-ground lightning strikes in the storm coincided with the occurrence of large hail.

1. Introduction

Weather forecasters who monitor and interpret radar data for issuance of severe thunderstorm warnings frequently observe that an echo develops a U- or V-shape when it is in the process of splitting. A storm splits into a rightmoving storm and a leftmoving storm because new updrafts develop on the storm's right and left lateral flanks (e.g., Charba and Sasaki 1971; Brown and Meitín 1994). Then, through a process of discrete propagation, the two updraft regions move away from each other as one or both storms become severe. However, on less frequent occasions, a storm is observed to maintain a V-shape (open in downstream direction) without splitting, such as the German hailstorm studied by Höller et al. (1994). By tracking reflectivity maxima, they noted that the wings of the V-shape generally corresponded to the tracks of the maxima. The reasons why reflectivity maxima would have divergent tracks within a given storm are not fully understood.

It is fortuitous that, during the 1989 North Dakota Thunderstorm Project (Boe et al. 1992), detailed single-Doppler radar data were collected in two non-splitting multicell storms that had V-shaped echoes. Brown et al. (2002) discuss cloud-to-ground lightning activity in relation to evolution of the V-shaped Elgin, North Dakota storm. In this two-part study, radar reflectivity and Doppler velocity signatures are used to investigate the structure and evolution of the companion Carson, North Dakota storm. In Part I of the study, updraft and hail evolution are deduced from Doppler radar measurements and the reason for the V-shape is revealed. In Part II, the midaltitude wake flow downstream of the updraft region will be investigated using Doppler velocity signatures.

An informative approach for depicting evolution of an individual radar cell within a convective storm is to plot a time-height profile of maximum reflectivity within observed cells (e.g., Renick 1971; Heymsfield 1981; Knight et al. 1983; Dye et al. 1986; Tuttle et al. 1989; Hondl and Eilts 1994; Brown et al. 2002) as well as within numerically modeled cells (e.g., Danielsen et al. 1972; English 1973). These profiles typically show radar-detectable particles initially forming at midaltitudes. With time, radar reflectivity increases in vertical extent, reaching the rising updraft summit and coincident cloud top. During the same time period, reflectivity intensity increases at midaltitudes as hydrometeors (typically graupel and/or hail) grow in size and concentration within the developing updraft. When midaltitude particles within the cell attain a sufficient size, such that the local updraft can no longer suspend them, they start to descend. As the reflectivity maximum reaches the ground, heavy rain, graupel and/or hail, and strong outflow winds may be observed at the surface. Meanwhile, following updraft demise, hydrometeors that had reached upper portions of the updraft within the cell take tens of minutes to fall out at their respective terminal velocities as they move downstream with the environmental flow. This updraft/downdraft cell evolution follows the general model proposed by Byers and Braham (1948) based on

data collected during the Thunderstorm Project of 1946-47.

As pointed out by Brown et al. (2002), the term "cell" has been misapplied in recent years. Instead of being applied to an individual updraft/downdraft cycle, the term is being applied to a cluster of cells, in various stages of updraft development, which is found in the middle- and upper-altitude maximum reflectivity region of a thunderstorm. It is easier to identify the overall cell cluster (maximum reflectivity region) than to identify the individual cells (localized reflectivity maxima and protrusions). For example, algorithms, such as the WSR-88D Storm Cell Identification and Tracking Algorithm (e.g., Johnson et al. 1998), identify the entire maximum reflectivity region as a cell.

Lacking dual-Doppler data, updraft locations in the Carson storm were deduced not only by using tops of rising reflectivity maxima as described above, but also by using collocated Doppler velocity signatures of surface convergence and storm-top divergence [single-Doppler velocity signatures are discussed by Brown and Wood (1991), among others]. These criteria, when observed simultaneously, define an updraft signature. This technique for locating updrafts, used to a limited extent by Brown and Meitín (1994), was developed more fully for this study of the Carson storm and for the Brown et al. (2002) study of the companion Elgin storm.

The types of data used in this study and the environmental setting in which the Carson storm formed are presented in section 2. Evolution of individual cells based on reflectivity and Doppler velocity signatures is discussed in section 3. Stages of storm development are outlined in section 4. The use of flare echoes to deduce the presence of hail is discussed in section 5. Cloud-to-ground lightning activity during the hail portion of the storm is examined in section 6. The reason for the storm's V-shaped structure is disclosed in section 7.

2. Data Sources and Environmental Setting

The Carson, North Dakota, multicell hailstorm occurred on the evening of 11 July 1989 during the North Dakota Thunderstorm Project (NDTP). The NDTP was conducted from 12 June through 22 July 1989 in south-central North Dakota. Its purpose was to study the dynamic and microphysical characteristics of northern Great Plains convective storms (Boe et al. 1992). Among the data collection platforms used in the project were six instrumented aircraft, Wave Propagation Laboratory's 5-cm-wavelength NOAA-C Doppler radar and the North Dakota rain and hail reporting network. In addition, the National Center for Atmospheric Research (NCAR) supplied two Cross-Chain Loran Atmospheric Sounding System (CLASS) rawinsonde systems, two Portable Automated Mesonet (PAM) sites, and CP-3 and CP-4 5-cm-wavelength Doppler radars (forming a dual-Doppler network). The CP-3 radar was located next to the Bismarck airport and the CP-4 radar was located 56 km to the northwest of CP-3 (Fig. 1). The North and South Dakota portions of the National Lightning Detection Network (NLDN) became operational in time to use for the project (e.g., Orville 1991). Surface observations and

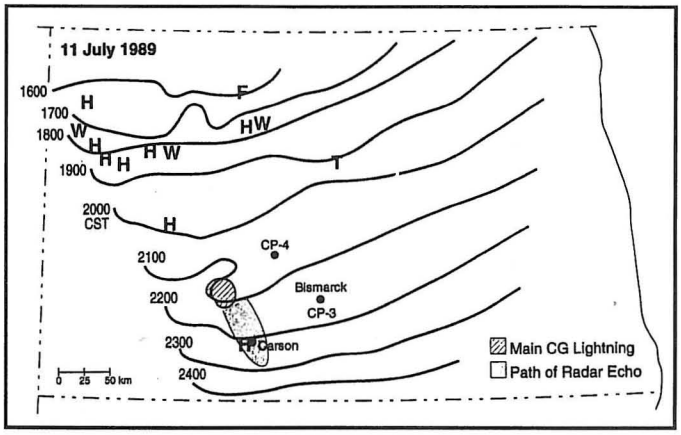

Fig. 1. The isochrones (solid lines, CST) represent the location in time and movement of the leading anvil edge of a convective line across North Dakota as determined from GOES-7 visual and infrared images. Hatched region is where most of the Carson storm's cloud-to-ground lightning activity occurred (prior to CP-3 data collection) and the shaded region is the path of the storm based on CP-3 radar data. Heavy dots represent locations of CP-3 and CP-4 radars. Letters represent reported weather events: H-hail ($\geq$ 1.9 cm), W-winds ($\geq$ 26 m s^{-1}), F-funnel cloud, and T-tornado (adapted from NCDC 1989).

routine 0600 and 1800 CST (all times in this paper are local Central Standard Time) rawinsonde releases from the National Weather Service (NWS) Forecast Office in Bismarck were incorporated into the project data set. GOES-7 visual and infrared satellite data provided an overview of convective storm activity.

Of the two NCAR Doppler radars, only CP-3 was used for this study of the Carson storm; CP-4 started to collect data as the storm was dying. The CP-3 radar completed sectorized scans through the storm in 3-5 min, with a new three-dimensional scan starting every 4-7 min. Twenty-two volume scans were collected between 2152 and 2400 CST. To study storm evolution at consistent heights, CP-3 Doppler velocity and reflectivity data were interpolated to a three-dimensional Cartesian grid using the NOAA/National Severe Storms Laboratory's Multiple-Doppler Radar Analysis (RADAN) System (e.g., Brown et al. 1981). Prior to interpolation, radar data within each three-dimensional volume scan were adjusted to a common reference time in order to correct for storm motion during the 3-5 min of data collection. Owing to the inherent smoothing nature of data interpolation, isolated extreme radar reflectivity values typically decreased by 1-6 dBZ. Similarly, the magnitude of extreme Doppler velocity values decreased by a few meters per second.

During the middle of the afternoon on 11 July 1989, a line of convection became organized in northwestern North Dakota (Fig. 1). There were several reports of severe weather activity (NCDC 1989). With westerly flow aloft, project personnel expected severe weather to remain north of the project area, so they ceased operations for the day around 1745 CST. However, the line had started to move south-southeastward by the time operations were terminated. Based on satellite images and tracks of cloud-to-ground lightning strikes, the Carson storm likely formed ahead of the line shortly after 2000

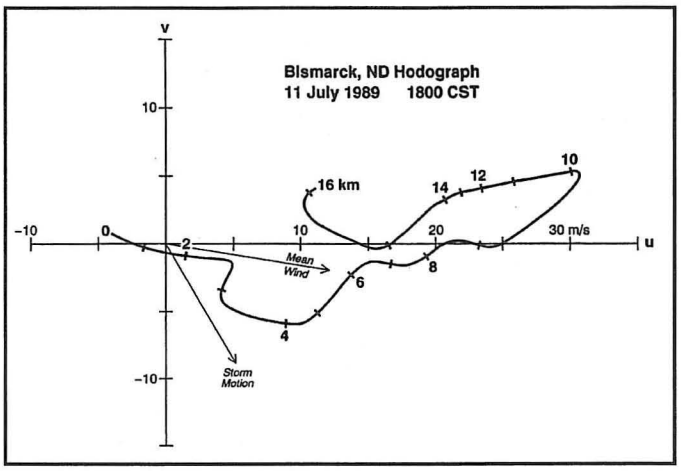

Fig. 2. Hodograph of ground-relative winds based on the 1800 CST 11 July 1989 rawinsonde launch by the National Weather Service in Bismarck, North Dakota. Bold numbers and hash marks represent altitudes AGL (km). Thin arrows represent LCL-EL mean wind and storm motion vectors. The winds in the lowest 1 km were adjusted to agree with the observed surface wind at that time.

CST. After the storm's existence became evident (visually and in the lightning network data), the CP-3 radar commenced data collection at 2152 CST (reference time of first volume scan is 2154 CST). Most of the time, the storm was over sparsely-populated areas. However, when the storm passed over the small community of Carson, there were reports of up to baseball-size hail in the general area starting at 2235 CST and lasting for 15 min (NCDC 1989).

Surface winds ahead of the convective line were generally light from the east and southeast. With height, winds shifted to westerly in response to the presence of an upper-level ridge that dominated much of the United States. The environmental sounding closest to the Carson storm was the NWS 1800 CST release at Bismarck. The sounding represents environmental conditions 2-3 hours before the storm formed and 50-75 km east of the storm's eventual track. Figure 2 shows the hodograph from that sounding. The mean wind was 12.4 m s^{-1} from 279°, computed as the mean of the winds at 50-hPa intervals from the lifting condensation level (800 hPa, 1.6 km above the ground) to the equilibrium level (250 hPa, 10.4 km). The mean shear vector over the same depth was 3 x 10^{-3} s^{-1} toward 083°. Individual convective cells within the storm moved generally in the direction of the mean wind. However, overall storm motion was from 330° at 10.3 m s^{-1}, propagating about 50° to the right of the mean wind. Curiously, the German hailstorm with the V-shaped reflectivity pattern studied by Höller et al. (1994) also propagated roughly 50° to the right of the mean wind at the time of the V-shape.

3. Evolution of Radar-Deduced Cells in the Carson Storm

Owing to the availability of only one Doppler radar for this study, reflectivity and Doppler velocity signatures were used to deduce evolution of updraft/downdraft cells. A cell is most obvious when it is at its greatest vertical extent. In plan view, the cell is characterized at mid- and upper altitudes by a reflectivity maximum or by a protrusion in the maximum reflectivity contours. These features are most prominent when reflectivity contours are presented at 2 dBZ intervals. By keeping track of the reflectivity maximum in the vertical and forward and backward in time, one develops a four-dimensional history of the reflectivity feature. One such history of maximum reflectivity associated with reflectivity feature 9R4 is shown in Fig. 3. [Each recognizable reflectivity feature (i.e., updraft/downdraft cell) in the Carson storm was given a three-component identifier. The first number represents the order in which the feature formed during the data analysis period. The number is followed by either an R or an L denoting whether it moved down the right (southern) or left (northern) flank of the V-shaped radar echo. The final number is the order in which the reflectivity feature moved down that particular flank.]

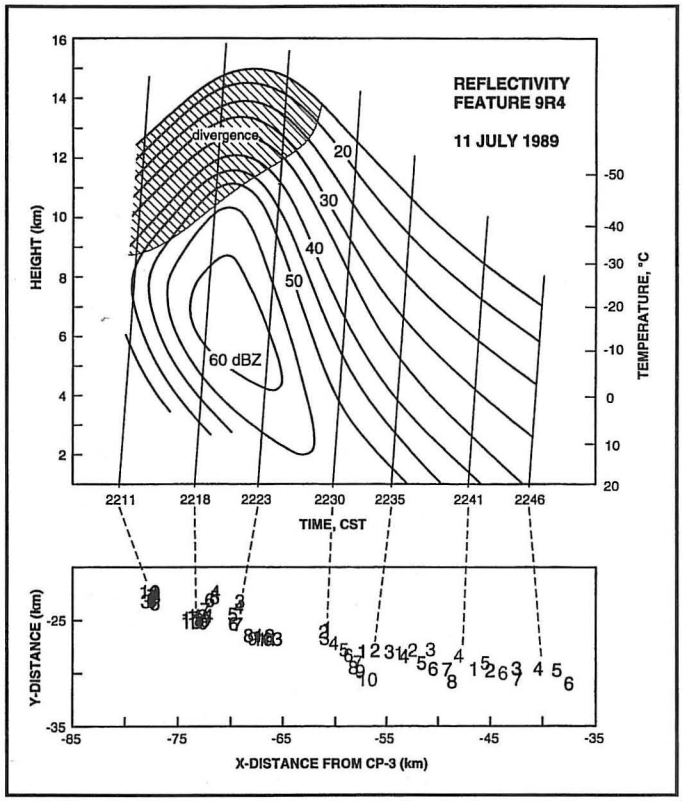

Fig. 3. This is a four-dimensional depiction of reflectivity feature 9R4. The top portion of the figure is a time-height plot of the feature, with contours of reflectivity (dBZ). Angled vertical lines represent data collection as a function of height and time for a given radar volume scan. Horizontal axis is time (CST), vertical axes represent height AGL (km) and environmental temperature (°C). Maximum reflectivity values were plotted at 1-km height increments and then the smoothed contours were drawn. Hatched area indicates times and heights where single-Doppler velocity signatures of divergence were detected. The bottom portion of the figure shows the projection of 9R4 data points onto a horizontal (x-y) plane. Location of the number denotes the projected location of the center of the feature; the number represents height in km. Each dashed line connects the reference time of the volume scan above with the corresponding projected data points.

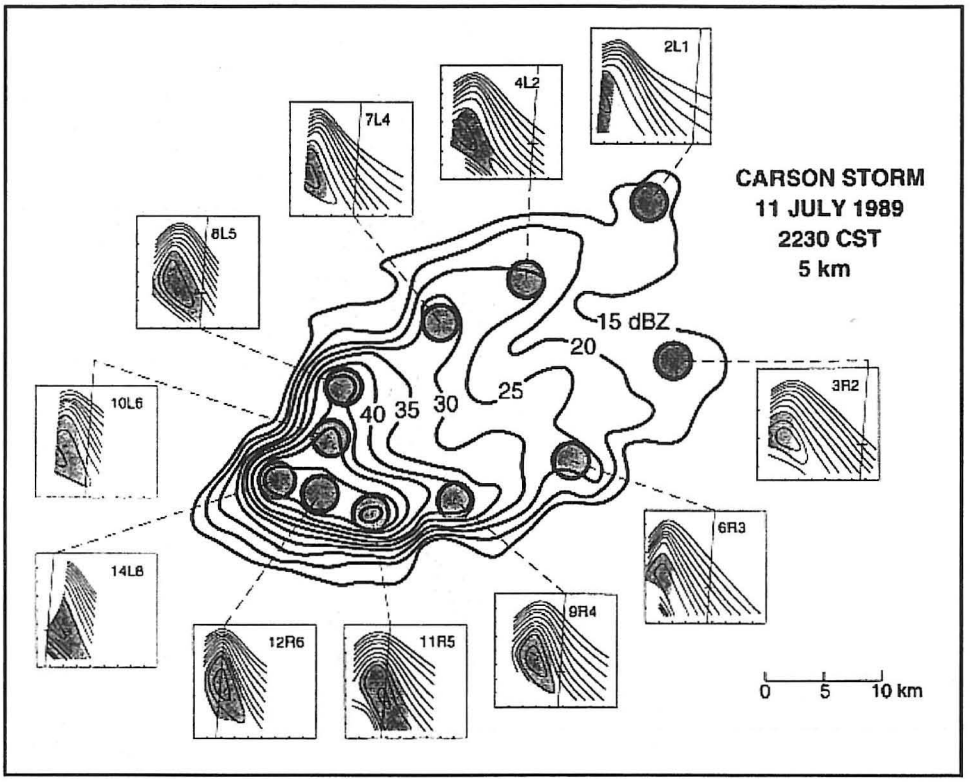

Fig. 4. Horizontal cross-section of radar reflectivity is shown at 5 km height at 2230 CST 11 July 1989. Solid contours are reflectivity (dBZ). Shaded circles indicate the locations of reflectivity features; corresponding time-height plots (abscissa is time [45 min] and ordinate is height [0-16 km]) of each are shown. The shaded areas in the time-height plots indicate the presence of hail flare echoes (discussed in section 5). The angled vertical line (with tick mark at 5 km height) in each plot indicates the position of the 2230 CST volume scan relative to cell lifetime.

At the earliest time of detection, feature 9R4 was barely detectable as it emerged from stronger reflectivities associated with the mature updrafts in existence at that time. With time, reflectivity values increased at all heights until feature 9R4 reached its maximum vertical extent. During this period, the strongest values remained at midaltitudes, suggesting that hydrometeors there were growing hailstones. Hydrometeors evidently became so large that they started to descend as the updraft and echo top were reaching their maximum vertical extent.

Reflectivity contours near the top of 9R4 ascended until about 2222 CST (Fig. 3). Contours ascending with time are evidence of an updraft in which precipitation particles are being produced and carried upward. Presence of an updraft is also indicated by Doppler velocity signatures of divergence in the upper portion of the cell and convergence near the ground. For most cells in the Carson storm, divergence near storm top was evident for approximately 4-6 minutes after the top of the reflectivity feature began its descent. With decreasing support for the updraft at lower levels, upward velocities eventually ceased and the divergence pattern disappeared. Descending contours (after time of maximum reflectivity at a given height) are evidence of precipitation particles descending toward the ground.

The lower portion of Fig. 3 shows the projection onto a horizontal plane of the centroid of reflectivity feature 9R4 at all heights and times. The location of each number on the horizontal plane denotes the horizontal projection of the center of the reflectivity feature, while the number itself indicates the height (km) above the ground at which this feature was detected. While the updraft was growing, the reflectivity feature was oriented essentially vertically. However, as the reflectivity feature (updraft portion of cell) was reaching its maximum vertical extent, it started to tilt to the right (i.e., south) with height signaling already at this stage that hydrometeors associated with 9R4 would be moving down the storm's right flank. With time, tilt of the associated reflectivity feature eventually shifted to the downstream (or east-southeasterly) direction and the feature moved more quickly toward the east-southeast in response to environmental winds that increased in speed with height. In contrast, a reflectivity feature that would move down the left flank of the storm would start to tilt to the left with height as it reached maximum vertical extent and then tilt toward an easterly downstream direction after updraft demise.

The nearly vertical orientation of the reflectivity feature during updraft growth attests to the ability of a strong updraft to remain vertical, even under the influence of mid- and upper-altitude shear. Similar results have been observed in other multicell hailstorms. For example, Dennis et al. (1970) reported, "Observers on the ground and in aircraft were in general agreement that most active cells were almost vertical . . . Only in their dissipating stages did the storm cells yield to the ambient wind shear and show a pronounced slope."

Keeping track of the same reflectivity feature in space and time, however, was not always a straightforward matter. When new radar cells developed in close proximity to older cells, separating the contribution of two or more reflectivity features within the high reflectivity region of the storm was sometimes difficult. This was complicated by apparent rapid growth of new updrafts during the most intense stage of the Carson storm, which was sampled coarsely by 5-6 min time intervals between successive volume scans. However, through the reflectivity analysis technique used here, if a reflectivity feature was improperly identified, reflectivity contours in the time-height plot (top of Fig. 3) would start rising again following initial descent. This situation indicated that one had started to track the wrong reflectivity feature. One also could tell that the wrong feature was being tracked when horizontal projections of the feature did not follow the type of evolution indicated in the bottom of Fig. 3.

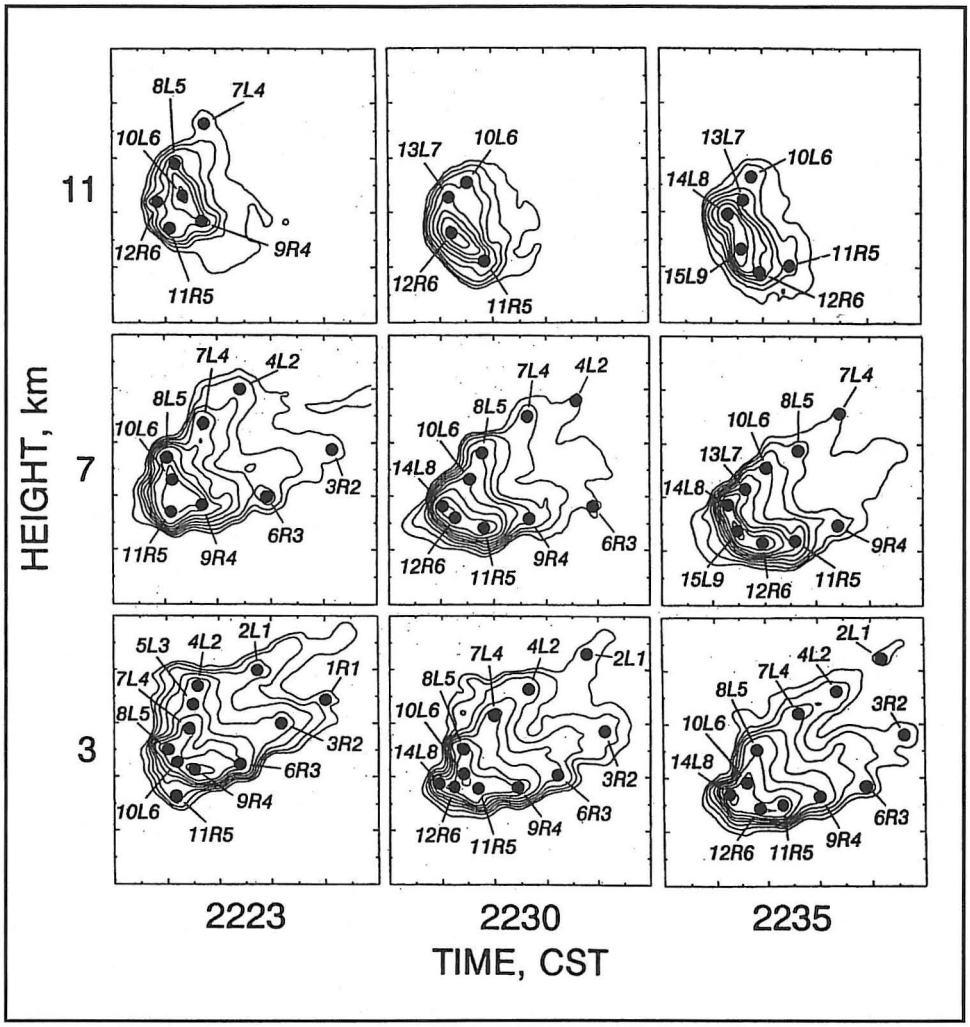

Fig. 5. Horizontal cross-sections of radar reflectivity (solid, dBZ) at 3, 7, and 11 km AGL for 2223, 2230, and 2235 CST 11 July 1989. Black dots are reflectivity maxima/protrusions. Displayed contour interval is 5 dBZ starting with 20 dBZ. Each box is 50 km by 50 km with the lower left corner located 85 km west and 35 km south of CP-3 radar.

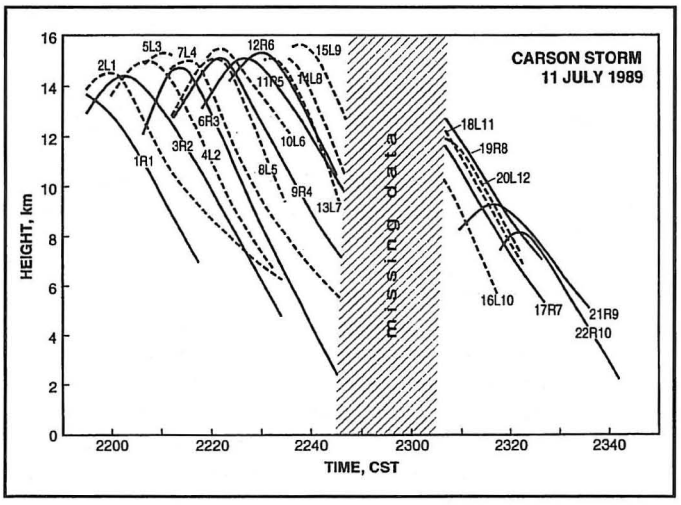

Fig. 6. Time-height plot of the 15-dBZ tops of reflectivity features within the Carson storm. Solid (dashed) contours indicate reflectivity (dBZ) features that moved down the right (left) flank. Hatched region represents missing data due to a power failure.

During the period of data collection, every cell within the Carson storm underwent the same type of evolution shown in Fig. 3. This fact is illustrated in Fig. 4, which shows time-height plots of the 11 cells/features identifiable at 5 km height in the storm at 2230 CST. The angled vertical line in each time-height plot indicates stage of cell evolution associated with each maximum or protrusion in the horizontal reflectivity pattern at reference time 2230 CST. Features 2L1 and 3R2 are nearing the ends of their lifetimes, with settling hydrometeors having about 6 km more to descend. Features 4L2, 6R3, and 7L4 are at earlier stages of descent. Shading within each plot indicates when hail was present in the cell as deduced by the presence of flare echoes in the radar reflectivity pattern (see discussion in section 5). Based on the shading, hail associated with feature 9R4 should have just ended at the surface, while hail associated with features 8L5 and 10L6 should have been in the process of ending. Hail associated with features 11R5 and 12R6 should be just arriving at the surface; based on reflectivity patterns in the time-height plots, the associated updrafts in the upper parts of the cells should be in the process of dying. The updraft associated with the newest feature, 14L8, likely is at its peak strength, even though the feature is not yet identifiable in the upper portion of the storm; hail evidently has not yet reached the ground from this cell.

The presentation in Fig. 4 indicates that the overall radar reflectivity pattern associated with a storm is produced by blending of hydrometeors that form in, and are carried aloft by, a series of updrafts. After a given updraft dies, the associated hydrometeors descend at their respective terminal velocities. Even though the hydrometeors become dispersed owing to vertical shear of the horizontal wind, the associated reflectivity maximum/protrusion remains identifiable for the 30-60 min it takes for the hydrometeors to reach the ground. It is the propensity for hydrometeors associated with a given updraft to remain identifiable, even after updraft demise, that has made it possible to take advantage of the reflectivity feature analysis technique used in this study.

Figure 5 shows evolving locations of all identified features in the Carson storm reflectivity field from 2223 to 2235 CST at 3, 7, and 11 km above ground level (AGL). Each reflectivity feature originated on the western end of the storm. At 2223 CST, for example, feature 12R6 was first detected from 9 to 14 km AGL. By 2230 CST, 12R6

was identifiable from 3 to 15 km with reflectivity values increasing to greater than 55 dBZ in the upper part of the storm as the associated updraft carried hydrometeors toward storm top. By 2235 CST, the top of feature 12R6 had begun to descend and had started to move down the southern (right) edge of the storm, signifying demise of the updraft. The other reflectivity features in the Carson storm underwent similar evolutions.

Based on identified reflectivity features in Fig. 5, successive features alternated in a somewhat orderly manner between the left and right flanks. If one considers the first 15 features (most of which are seen in Figs. 4 and 5), the order of movement was R, L, R, L, L, R, L, L, R, L, R, R, L, L, L. The "V-shaped" pattern apparent in the reflectivity contours at mid- and low altitudes is due to this alternate movement of updraft-produced hydrometeors down either the right or left flank. The likely reason for the alternating behavior is discussed later in section 7.

In all, 22 reflectivity features associated with updraft/downdraft cells were identified during the data collection period. Time-height histories of the 15-dBZ tops of these features are plotted in Fig. 6. For example, the 9R4 curve in Fig. 6 is the same as the uppermost contour (15 dBZ) in the top portion of Fig. 3. Between reference times 2154 and 2246 CST, reflectivity features generally grew to increasingly greater heights. Feature 15L9 was the tallest, reaching a 15-dBZ height of 15.6 km. During this period, new updrafts formed at increasingly frequent intervals. In fact, formation of new updrafts between 2241 and 2246 CST was so frequent that it was difficult to identify new reflectivity features. Note that features 13L7, 14L8, and 15L9 were not identifiable until they were at or just beyond their maximum vertical extent. The identification difficulty was due to two factors: (a) the average time interval of 5-6 minutes between volume scans and (b) the period of missing data following the 2246 CST volume scan. A couple of new features (not shown in Fig. 6) that appeared between 2235 and 2246 CST were not numbered because the missing data gap prevented their spatial and temporal continuity from being satisfactorily resolved.

Just before 2250 CST, there was a power outage at the radar site. CP-3 radar resumed operation at 2305 CST, by which time the storm had weakened considerably. As the storm died, new updrafts were still being produced, but each successive one grew to lower and lower heights. Evidently the low-altitude discontinuity that triggered new updrafts was still present, but air flowing into the new updrafts was becoming more stable. The updraft associated with feature 22R10 was the last one detectable within the storm, reaching a height of only 8 km. The process of successive updrafts growing to greater and greater heights, reaching maximum vertical extent, and then growing to lesser and lesser heights is reminiscent of deduced updraft evolution in two multicell storms studied by Brown and Meitín (1994).

In summary, it is reasonable to assume that updrafts in the Carson storm formed along a gust front that was undetectable by radar owing to the storm's distance from the radar. The following chain of events is assumed to have been associated with the demise of each

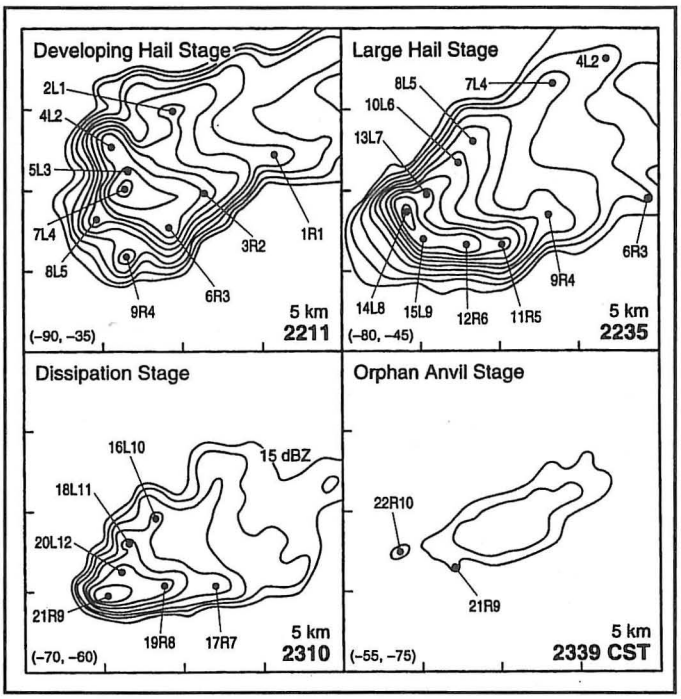

Fig. 7. This is a sample of horizontal reflectivity fields at 5 km height during four stages of development in the Carson storm. Reflectivity contours (solid) are at 5-dBZ intervals beginning with 15 dBZ. Dots indicate the centers of labeled reflectivity features. During the Dissipation Stage, features in the eastern portion of the radar echo were not identified because continuity of features was lost during a period of missing data from 2250 through 2305 CST. Border tick marks indicating the distance from the CP-3 radar are at 10-km intervals starting with the (x, y) values in the bottom left corner. Bold numbers in bottom right corners indicate time in CST 11 July 1989.

updraft/downdraft cell. As the gust front moved southward, convergence associated with it moved away from the base of existing updraft. With no mechanism to continue upward transport of momentum through the lower portion of the updraft, coupled with increasing precipitation loading at midaltitudes, upward velocities in the updraft weakened and disappeared. With support no longer present, all hydrometeors that had formed in the updraft and been carried aloft began to descend to the ground. One could follow these descending columns of precipitation as distinct protrusions for over 30 minutes as they moved downstream through the storm in response to ambient flow.

4. Stages of Storm Development

Six main stages of development in the Carson storm were identified from the various data sources. These stages and their approximate times of existence are:

Initial Growth Stage	2015 - 2039 CST
CG Lightning Stage	2039 - 2143 CST
Developing Hail Stage	2143 - 2217 CST
Large Hail Stage	2217 - 2250 CST
Dissipation Stage	2250 - 2325 CST
Orphan Anvil Stage	2325 & beyond

Based on lightning and satellite data, it is estimated that the storm formed at roughly 2015 CST. The Initial Growth Stage, prior to Doppler radar data collection, is taken to be that period of the storm's initial development prior to the first detected cloud-to-ground (CG) lightning strike. The CG Lightning Stage, also prior to the start of radar data collection, is a 64-min period dominated by 36 CG strikes (all negative).

The four remaining stages occurred primarily during the time period of Doppler radar data collection that commenced at 2152 CST. Typical reflectivity patterns during these four stages are shown in Fig. 7. The Developing Hail Stage is defined as the period during which the hail flare echo was growing in radial and vertical extent (see sections 5 and 6). At 2211 CST in Fig. 7, five reflectivity features (5L3, 6R3, 7L4, 8L5, and 9R4) at the upstream end of the storm were at various stages of updraft development. Three features were in the main reflectivity core region and two of them were forming upstream of the others. During this stage, there was a marked decrease in CG lightning activity. One negative ground strike occurred next to the updraft/hail-growth region and three negative strikes occurred beneath the downstream anvil.

It is assumed that the Large Hail Stage began soon after maximum flare echo length exceeded 20 km and ended when the last reported large hail occurred on the ground (shown later in Fig. 11). Hailstones up to golf ball and baseball in size were reported on the ground at 2235 CST and hailfall continued for about 15 min. The three positive cloud-to-ground strikes associated with the storm occurred during this stage within or at the downstream edge of the convective region (defined as reflectivities greater than 40-45 dBZ). The reflectivity pattern at 2235 CST (Fig. 7) shows a much more organized distribution of reflectivity features during this stage. The overall reflectivity pattern is in the shape of a U or V. During this stage of storm development, it was typical for only one, or briefly two, updrafts to be in existence at a given time, with the newest updraft being along the upstream edge of the echo.

During the Dissipation Stage, updrafts continued to form within the storm, but they had less energy and each successive one grew to lower and lower heights (see Fig. 6). These weaker updrafts apparently continued to produce small hail because hail flare echoes were observed, but length and vertical extent of the echoes decreased with time. The last flare echo, associated with feature 22R10, was observed only during the 2324 CST volume scan. There was no recorded CG lightning activity during this stage.

The final stage of storm evolution is called the Orphan Anvil Stage. Except for precipitation cores (associated with identifiable reflectivity features) settling out at lower altitudes, all that remained was a nondescript three-dimensional plume of radar echo. The plume extended 50-100 km downstream from where the storm's updraft region had been. At low altitudes, the upstream end of the plume coincided with the descending precipitation cores. With increasing altitude, the upstream end tilted downstream, as it responded to stronger winds aloft. The orphan anvil drifted downstream and unquestionably disappeared after all hydrometeors had either settled out or sublimated/evaporated.

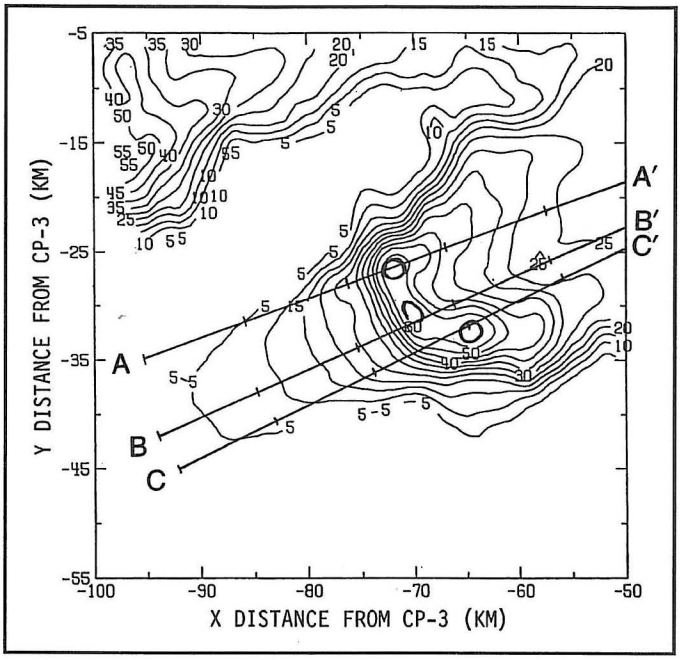

Fig. 8. Horizontal cross-section of radar reflectivity (solid, dBZ) is shown at a height of 6 km at 2235 CST 11 July 1989. Lines AA', BB', and CC' are radial lines from the radar that indicate the locations where the vertical cross-sections in Fig. 9 pass through the three-dimensional centroids of reflectivity features 14L8, 15L9, and 12R6, respectively. The small bold closed contours indicate the locations of the features at 6 km height. Tick marks along each line are at 10-km intervals from the left end of the line.

5. Hail Flare Echoes in the Carson Storm

Throughout much of the Doppler radar collection period, a prominent phenomenon known as a "flare echo" (e.g., Wilson and Reum 1988; Nielsen-Gammon and Read 1995; Lemon 1998) was noted in the reflectivity field of the Carson storm. Zrnic (1987) defined the flare echo or "hail spike" signature as a three-body scatter process that arises from strong non-Rayleigh scattering by large hydrometeors, especially water-coated hailstones. Radar radiation is scattered in all directions from the hail region, with only a small amount of this radiation being backscattered to the radar (producing the commonly-recognized storm echo). Other radiation is scattered toward the ground. Radiation that reaches the ground undergoes a second scattering process in which energy is scattered skyward in all directions. A portion of this energy again encounters hail within the hail region in the storm and is scattered a third time in all directions. Some of this much weaker energy also reaches the radar. Since this energy arrives at the radar later than energy initially scattered by the hail, the radar processor assumes that this scattered energy originated beyond the hail region at the same elevation angle. If the hail region is near the far edge of the storm relative to the radar, a flare echo extends beyond the storm echo; if the hail region is near the near edge of the storm relative to the radar, the flare echo usually is obscured by the stronger reflectivity portion of the storm.

The shortest path traveled in the three-body scatter process is from the hail region vertically down to the ground and vertically back up to the hail region and then

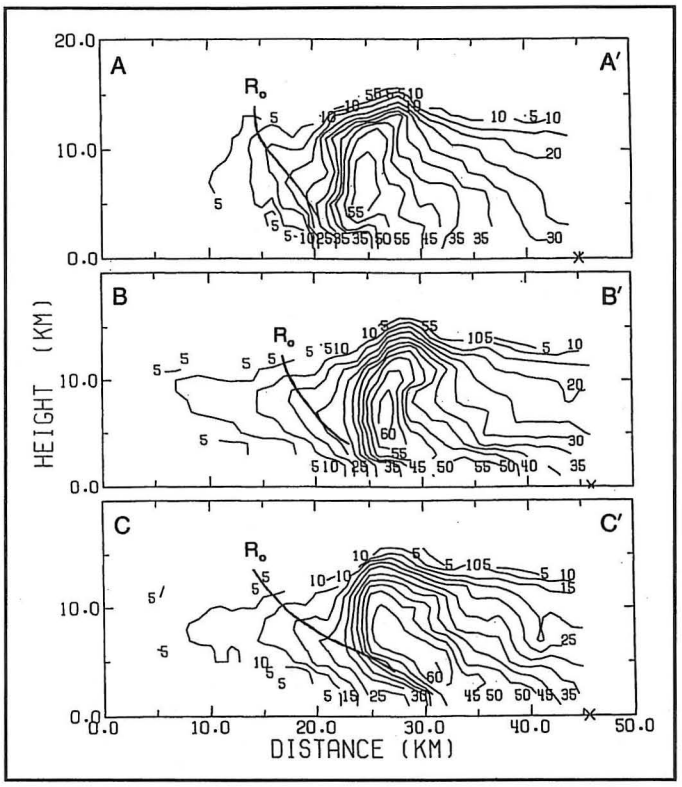

Fig. 9. Vertical cross-sections of storm and flare echo reflectivities (solid, dBZ) along the three radial lines shown in Fig. 8. The curves labeled R_0 (representing the nominal beginning of the flare echo) are at the same distances from the centers of the reflectivity features as the corresponding elevation angles are above the ground beneath the features. Distance is measured relative to the left end of lines AA', BB', and CC' in Fig. 8.

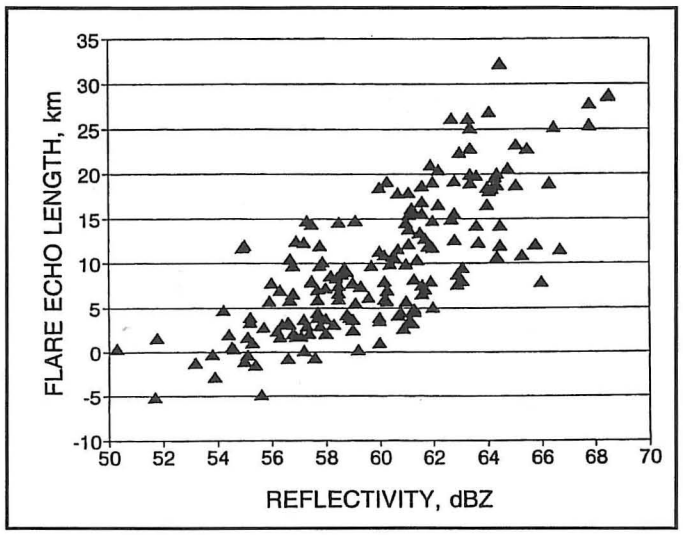

Fig. 10. Scatter diagram of hail flare echo length (km) versus maximum reflectivity (dBZ) at the center of the hail region at the same elevation angle. Flare echo length is the distance from the beginning of the flare echo (R_0) to the 3-dBZ end of the echo. Negative flare echo lengths, which all occurred at the highest elevation scans that produced flare echoes, suggest that scattering took place from the portion of the high reflectivity region closest to the radar rather than from the center, which was assumed for the computations. Likewise, some of the scatter in the diagram probably resulted from the estimation of hail flare length in relation to the center of the high reflectivity core when it should have been estimated from the closer or farther edge of the core region.

back to the radar. This path produces the shortest time delay, which means that the beginning of the flare echo appears radially beyond the associated reflectivity core region at a distance (R_0) equal to height of the core region above the ground. Zrnic (1987) derived the theoretical dependence of flare echo intensity on distance R along the scattering path to be $1/R^3$. Based on measurements in Alabama and Colorado flare echoes, Wilson and Reum (1988) confirmed that radar reflectivity changes as $1/R^3$ with distance from the radar. The strongest flare echo signal thus appears at the end of the flare echo located closest to the radar (i.e., at distance R_0 beyond the hail region).

The Carson storm was examined for all flare echo signatures and a data set was compiled using unsmoothed reflectivity fields replayed on a plan position indicator (PPI) display. The far end of the flare echo was defined as that point where the reflectivity value was 3 dBZ. A total of about 150 flare echo components were detected from the beginning of data collection through 2324 CST; a flare echo that extended in the vertical through a number of successive elevation angles was tabulated as a separate component at each elevation angle. When a couple of adjacent reflectivity features contributed to the same broad composite flare echo, the flare echo associated with each individual feature at that height was tabulated as a separate component.

Figure 8 shows a horizontal slice through the smoothed reflectivity field at a height of 6 km at 2235 CST. The flare echo appears as a broad protrusion extending about 20 km (based on the 5-dBZ contour) in a radial direction west-southwestward from the storm's high reflectivity core. Radial lines AA', BB', and CC' pass through the three-dimensional centroids of reflectivity features 14L8, 15L9, and 12R6, respectively. The blunt-nosed profile of the flare echo suggests that it was broadened by overlapping contributions from hail flare echo signatures associated with the three reflectivity features.

Vertical cross-sections of reflectivity along radial lines AA', BB', and CC' (Fig. 8) are shown in Fig. 9. The cross-sections clearly reveal the vertical extent of the flare echo extending to the left of the individual core regions. Superimposed on each cross-section is a curved line R_0 (minimum three-body scatter distance) that is plotted independently at the same slant range distance from the center of the reflectivity core as the height of the core above the ground. As mentioned, Zrnic's (1987) three-body scatter theory indicates that R_0 should be the beginning of the flare echo signature at a given elevation angle and it should be the location of the strongest reflectivity within the flare echo. Each R_0 curve in Fig. 9 coincides with the center of a local maximum in the contoured reflectivity pattern of the flare echo that evidently is the beginning of the flare echo. This observed relationship, along with similar observations by Wilson and Reum (1988) in Alabama and Colorado storms, helps to confirm Zrnic's hypothesis that the flare echo arises from three-body scattering.

From Zrnic's (1987) case study using a 10-cm Doppler radar, the flare echo was apparent when hail core reflec-

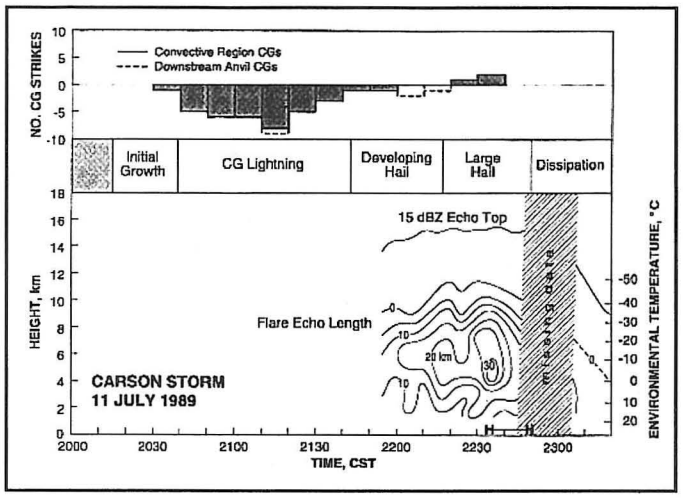

Fig. 11. *(Bottom)* Time-height cross-section of maximum flare echo length (km) and 15-dBZ storm top contour are shown. The dashed portion of the flare-echo-length contour is approximated. Duration of large hail reported at the ground near Carson is indicated by H's. *(Middle)* Stages of storm development with time are shown. *(Top)* Frequency of cloud-to-ground lightning strikes during 10-min intervals in the Carson storm are diagramed; data from the National Lightning Detection Network. Positive (negative) values indicate the number of positive (negative) CG strikes. Dashed lines indicate CG strikes beneath the anvil 40-50 km downstream of the storm's convective region.

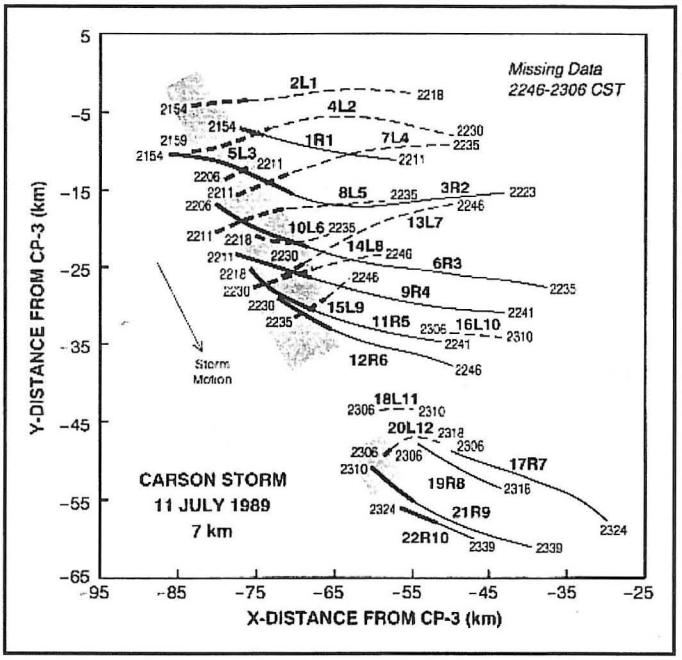

Fig. 12. Horizontal tracks of reflectivity features on x-y plane at a height of 7 km AGL. For example, the track labeled 9R4 was obtained by connecting the 7's in the bottom of Fig. 3. Beginning and ending times (CST) of each reflectivity feature are indicated. Left-flank (right-flank) features are indicated by dashed (solid) curves. Low-altitude convergence (shaded regions at west end of tracks) occurring beneath upper-altitude divergence (bold portions of tracks) adds additional credence to the existence of updrafts at the western end of the storm. Data are missing between the 2246 and 2306 CST volume scans due to power outage.

tivity values exceeded 57 dBZ. Using a 10-cm-wavelength WSR-88D radar, Nielsen-Gammon and Read (1995) similarly found that a Texas flare echo was detected when the maximum reflectivity core was 58 dBZ or more. Lemon (1998) found the WSR-88D threshold value to be about 63 dBZ for an Oklahoma hailstorm. In the Carson storm, the 5-cm-wavelength CP-3 radar detected flare echoes associated with reflectivity values as low as 50-53 dBZ. The scatter plot in Fig. 10 indicates that flare echo length is proportional to the magnitude of maximum reflectivity in the hail region. As pointed out by Wilson and Reum (1988), shorter wavelength radars produce more prominent flare echoes, owing to enhanced non-Rayleigh scattering associated with large hydrometeors.

6. Deduced Hail Evolution and Cloud-to-Ground Lightning Activity

Maximum length of the flare echo (from R_0 to the 3-dBZ end of the echo) at each elevation angle and for each volume scan is contoured in the bottom part of Fig. 11. Contours indicate that, at the time CP-3 data collection commenced (2152 CST), the flare echo - with significant hail likely associated with it - had just started to form in the storm; the flare echo probably appeared around 2143 CST (indicating beginning of the Developing Hail Stage). Hail forming in successive updrafts likely grew to progressively larger sizes for the next 50 min. Using flare echo length as an indication, the largest hail presumably appeared aloft in the storm between 2230 and 2240 CST. Golfball to baseball-size hail was first reported at the ground in the vicinity of Carson at 2235 CST. By the time the hail ended about 15 min later, hail up to 30 cm deep in some places covered a 50 km^2 area to the west of Carson. Flare echo data in Figs. 4 and 11 indicate that, for a storm moving at 10 m s^{-1}, hail likely was occurring along much of a 30-km-long, sparsely populated swath before producing obviously larger hail (based on maximum hail flare length) in the vicinity of Carson. According to *Storm Data* (NCDC 1989), crops, trees, vehicles, and buildings near Carson sustained hundreds of thousands of dollars worth of damage.

Cloud-to-ground lightning strikes associated with the Carson storm are summarized in the top portion of Fig. 11. Most of the negative CG lightning activity occurred during the CG Lightning Stage from 2039-2143 CST. There was a concentration of 15 CG strikes during the 15-min period from 2109 to 2124 CST. CG lightning activity likely was associated with localized rainfall reports along east-west Interstate 94 about 60 km northwest of Carson, where the storm would have crossed about 2100 CST as it moved southeastward toward Carson. There were no reports from the North Dakota rain and hail reporting network that hail was occurring there during that time period.

By the time that the Doppler radar started collecting three-dimensional volume scans at 2152 CST, CG activity had decreased significantly. A CG strike at 2157 CST occurred at the edge of the storm's convective region (radar reflectivity values greater than 40-45 dBZ). It was the last negative strike to occur in the convective region.

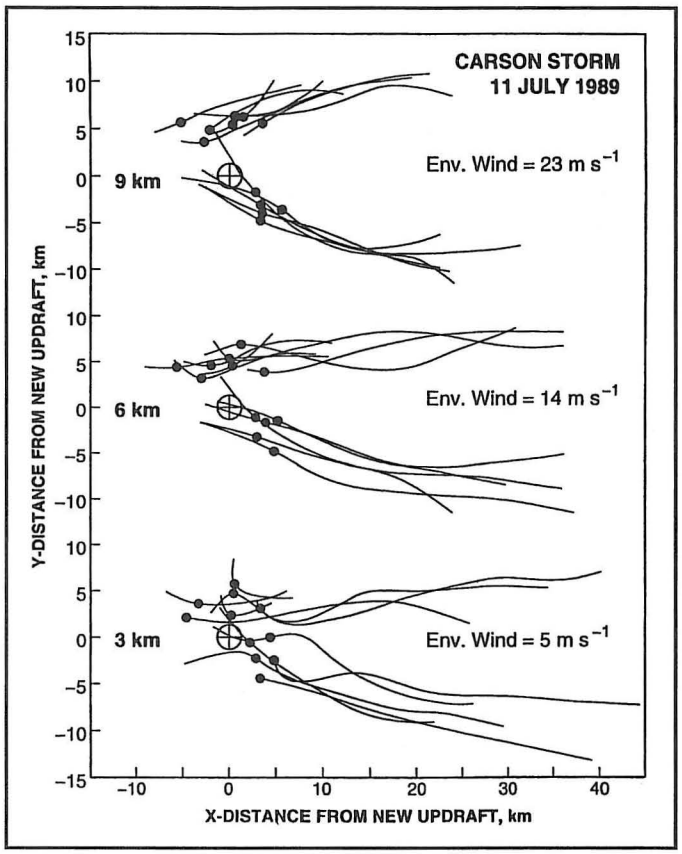

Fig. 13. Composite tracks of reflectivity features are shown at three heights relative to the center of the newest feature/updraft (plus mark in circle). The center of the newest feature represents its location relative to each existing feature at the time (dot) that the latter was at its maximum vertical extent. Offset of the newest feature toward the south may be a consequence of storm propagation in that direction. Ground-relative environmental wind speed is indicated at each of the three heights.

The next CG strike (positive) in the convective region did not occur for another 25 min. However, between 2204 and 2214 CST, three negative strikes occurred beneath the anvil, 40-50 km downstream of the convective region. The only positive CG lightning strikes detected in the storm occurred at 2222, 2238, and 2240 CST. All three strikes took place within or at the downstream edge of the convective region immediately before and during the reported fall of baseball-size hail in the Carson area. No more CG strikes were produced by the storm after 2240 CST because successive updrafts had started to weaken and, correspondingly, hail production was coming to an end.

The results of this study are consistent with various statistical studies of the relationship between hail and positive CG occurrences. Studies such as those by Reap and MacGorman (1989), Stolzenburg (1994), and MacGorman and Burgess (1994) all found that positive CG strikes occurred predominantly with storms producing large hail.

7. Storm Evolution Resulting from Updraft Interactions with Ambient Flow

The horizontal tracks of all reflectivity features at 7-km heights are shown in Fig. 12. Although the Carson storm moved toward the southeast, overall motion of individual reflectivity features generally was toward the east to east-southeast, in basic agreement with the mean wind direction and the environmental wind at 7-km height (Fig. 2). However, during the updraft phase (growth portion of features indicated by shaded regions and bold portions of curves), those features that eventually moved down the right flank tended to initially move more toward the southeast. Those that eventually moved down the left flank initially moved more toward the east-northeast. It is as if the reflectivity feature associated with a given updraft was predestined to move down a particular side of the storm.

The predestined motion was likely a result of flow that a given updraft/reflectivity feature experienced. Tilting of a reflectivity feature toward the left or right began when the associated mature updraft started to weaken as it approached its maximum vertical extent (e.g., Fig. 3). Thus, it may be that the next newer updraft (which was too strong to be tilted by vertical shear of the wind) was perturbing ambient flow at the location of the mature updraft. To test this concept, the position of each reflectivity feature at the time that it was the tallest (when it was starting to tilt) was plotted relative to the next newer feature at the same time.

The plots in Fig. 13 show the location of the tallest portion of each cell (dot) relative to the nearby newer feature (plus mark in circle) at heights of 3, 6, and 9 km. Tracks of each of these cells are indicated. The resulting composite plots clearly indicate that the cells responded to flow around the newest updraft feature. The stronger the ambient flow (i.e., the greater the height above the ground) the greater the diffluent flow around the new updraft and the more coincident the relative tracks. With greater diffluent flow at higher altitudes, updrafts on the right side of the new updraft started tilting to the right with increasing height and those on the left side started tilting to the left. Responding to the diffluent flow with time, every cell on the right side of the new updraft moved down the storm's right flank and every cell on the left side moved down the left flank. Each successive updraft took its turn being the perturbator of the flow when it was strongest and then, as it weakened, it succumbed to the flow around the next strong updraft. It appears that each new updraft randomly formed to the left or right of the previous updraft. In this way, the radar echo maintained its V-shape.

8. Conclusions

The Carson, North Dakota, multicell hailstorm occurred on the evening of 11 July 1989 during the North Dakota Thunderstorm Project. Though the storm was monitored by only a single Doppler radar (NCAR's 5-cm-wavelength CP-3 radar), a great deal was deduced about storm evolution through the use of single-Doppler velocity and reflectivity signatures. Key points of this descriptive study are discussed below.

- Within the reflectivity field of the Carson storm, distinct individual reflectivity maxima or protrusions rep-

resented hydrometeors within growing updrafts and subsequent hydrometeor fallout. An ascending reflectivity feature, associated with single-Doppler velocity signatures of convergence near the ground and divergence in the upper few kilometers of the cell, was interpreted to be an updraft. A descending reflectivity feature was interpreted to be descending hydrometeors. Though identifying the reflectivity signatures (through four-dimensional continuity) was a tedious process, the use of these signatures produced rewarding results in understanding the overall structure and evolution of the Carson storm.

- All deduced updrafts formed on the western (upstream) end of the storm. Reflectivity features associated with them were vertical during the growth stage. Since a growing updraft was so strong that it was not significantly affected by ambient shear, upstream air was forced to flow around the updraft. The resulting diffluent flow affected the slightly older nearby updrafts. Those updrafts on the right side (south side) of the newest updraft started tilting and moving to the right and those on the left side started tilting and moving to the left. As the older updrafts weakened and died, the increase of ambient flow with height began tilting the associated reflectivity features in a more downstream direction with height. The resulting reflectivity pattern was in the form of a V with the point at the upstream end of the storm.

- The flare echo extending out the far side of the storm, relative to the radar, provided a reasonable indication that hail was being produced in the storm. Midaltitude flare echo length progressively increased during the first 40 min of data collection, suggesting that sizes and/or concentration of hailstones were increasing with time. If hailstone sizes were increasing in successive updrafts (which were getting successively taller and presumably stronger as indicated by the height of reflectivity features), then hailstone growth within a new updraft may have been getting a head start through recycling of embryos and/or small hailstones from older nearby cells. Midaltitude flare echo length was greatest when golf-ball- to baseball-size hail started to fall in the Carson area. Flare echo length then decreased as the storm subsequently weakened.

- Eighty percent of detected cloud-to-ground (CG) lightning strikes beneath the storm occurred during a 75-min period prior to collection of Doppler radar data. All of those strikes transferred negative charge to the ground. Only four CG strikes occurred in the storm's growth region during the time that flare echoes indicated the presence of hail. Three of these strikes, that were the only positive ones in the storm, occurred while golf-ball- to baseball-size hail was reported on the ground. The occurrence of positive CG strikes during the production of large hail is frequently observed (e.g., Reap and MacGorman 1989; MacGorman and Burgess 1994; Stolzenburg 1994).

Acknowledgments

This research was supported in part through Cooperative Agreement NA47RA0184 from the NOAA Federal-State Cooperative Program in Atmospheric Modification Research to the North Dakota Atmospheric Resource Board (NDARB). We are grateful for the continuing interest of Bruce Boe, past Director of the NDARB and Director of the North Dakota Thunderstorm Project. John Helsdon (South Dakota School of Mines & Technology) provided the inspiration for studying this storm by recognizing the storm's existence and calling in Bob Bowie and his crew (National Center for Atmospheric Research), who conscientiously collected the CP-3 radar data. John Hirsch (SDSM&T) provided sounding data. Bob Rilling (NCAR) kindly provided us with CP-3, PAM and CLASS data sets. Cristina Kaufman (lately of NCAR) assisted with the processing of lightning data. We appreciate the comments of Carl Hane, Pam Heinselman, and Ted Mansell (NSSL) on various versions of the manuscript. Joan O'Bannon (NSSL) ably prepared the figures. Reviewers Bradford Herold (Midwest Weather, Inc.) and Richard Dixon (Southwest Texas State University) provided many helpful suggestions for improving the manuscript.

Authors

Rodger Brown has been a research meteorologist at the NOAA/National Severe Storms Laboratory (NSSL) since 1970. He earned a B.S. degree in earth sciences from Antioch College, M.S. in geophysical sciences from the University of Chicago, and Ph.D. in meteorology from the University of Oklahoma. While an undergraduate student, he worked at the Mount Washington Observatory, Blue Hill Meteorological Observatory, U.S. Weather Bureau's Severe Local Storms Research Unit, and spent a year at Little America V, Antarctica with the Weather Bureau during the International Geophysical Year. In recognition of his Antarctic service, a 1.4 km tall peak in west Antarctica was named Mount Rodger. Before arriving at NSSL, he was a research meteorologist at Cornell Aeronautical Laboratory in Buffalo, New York and at the Wave Propagation Laboratory in Boulder, Colorado. At NSSL, Rodger has been involved with various aspects of Doppler radar ranging from (a) severe storm studies to (b) understanding of Doppler velocity signatures in severe storms through simulations to (c) development of refined WSR-88D scanning strategies to provide greater spatial and temporal resolution of severe storms. He has served as member and chair of the American Meteorological Society's Severe Local Storms Committee and has served the National Weather Association as Secretary, Vice President, Commissioner of Committees, and Councilor. He also served as Program Chair for the AMS 13th Conference on Severe Local Storms in 1983 and for the NWA Annual Meeting in 1989.

Kathleen Torgerson has been a forecaster with the NOAA/National Weather Service (NWS) at Pueblo, Colorado since 1998, where her program responsibilities include radar and the Interactive Forecast Preparation System. Previously, she worked as a meteorologist intern at NWS Pueblo, and NWS Denver, Colorado. She gradu-

ated from the University of Oklahoma in 1994, where she earned a B.S. in Meteorology. While an undergraduate student, she worked at the National Severe Storms Laboratory as a meteorologist technician.

References

Boe, B. A., and Coauthors, 1992: The North Dakota Thunderstorm Project: A cooperative study of High Plains thunderstorms. *Bull. Amer. Meteor. Soc.,* 73, 145-160.

Brown, R. A., and V. T. Wood, 1991: On the interpretation of single-Doppler velocity patterns within severe thunderstorms. *Wea. Forecasting*, 6, 32-48.

_____, and R. J. Meitín, 1994: Evolution and morphology of two splitting thunderstorms with dominant left-moving members. *Mon. Wea. Rev.*, 122, 2052-2067.

_____, C. R. Safford, S. P. Nelson, D. W. Burgess, W. C. Bumgarner, M. L. Weible, and L. C. Fortner, 1981: Multiple Doppler radar analysis of severe thunderstorms: Designing a general analysis system. NOAA Tech. Memo. ERL NSSL-92, Nat. Severe Storms Lab., Norman, 21 pp.

_____, C. A. Kaufman, and D. R. MacGorman, 2002: Cloud-to-ground lightning associated with the evolution of a multicell storm. *J. Geophys. Res.*, 107(D19), 4397, doi:10.1029/2001JD000968.

Byers, H. R., and R. R. Braham, Jr., 1948: Thunderstorm structure and circulation. *J. Meteor.*, 5, 71-86.

Charba, J., and Y. Sasaki, 1971: Structure and movement of the severe thunderstorms of 3 April 1964 as revealed from radar and surface mesonetwork data analysis. *J. Meteor. Soc. Japan*, 49, 191-214.

Danielsen, E. F., R. Bleck, and D. A. Morris, 1972: Hail growth by stochastic collection in a cumulus model. *J. Atmos. Sci.*, 29, 135-155.

Dennis, A. S., C. A. Schock, and A. Koscielski, 1970: Characteristics of hailstorms of western South Dakota. *J. Appl. Meteor.*, 9, 127-135.

Dye, J. E., and Coauthors, 1986: Early electrification and precipitation development in a small, isolated Montana cumulonimbus. *J. Geophys. Res.*, 91, 1231-1247.

English, M., 1973: Alberta hailstorms. Part II: Growth of large hail in the storm. *Meteor. Monogr.*, No. 14 (36), Amer. Meteor. Soc., 37-98.

Heymsfield, G. M., 1981: Evolution of downdrafts and rotation in an Illinois thunderstorm. *Mon. Wea. Rev.*, 109, 1969-1988.

Höller, H., V. N. Bringi, J. Hubbert, M. Hagen, and P. F. Meischner, 1994: Life cycle and precipitation formation in a hybrid-type hailstorm revealed by polarimetric and Doppler radar measurements. *J. Atmos. Sci.*, 51, 2500-2522.

Hondl, K. D., and M. D. Eilts, 1994: Doppler radar signatures of developing thunderstorms and their potential to indicate the onset of cloud-to-ground lightning. *Mon. Wea. Rev.,* 122, 1818-1836.

Johnson, J. T., P. L. MacKeen, A. Witt, E. D. Mitchell, G. J. Stumpf, M. D. Eilts, and K. W. Thomas, 1998: The storm cell identification and tracking algorithm: An enhanced WSR-88D algorithm. *Wea. Forecasting*, 13, 263-276.

Knight, C. A., W. D. Hall, and P. M. Roskowski, 1983: Visual cloud histories related to first echo formation in northeast Colorado cumulus. *J. Climate Appl. Meteor.*, 22, 1022-1040.

Lemon, L. R., 1998: The radar "three-body scatter spike": An operational large-hail signature. *Wea. Forecasting*, 13, 327-340.

MacGorman, D. R., and D. W. Burgess, 1994: Positive cloud-to-ground lightning in tornadic storms and hailstorms. *Mon. Wea. Rev.*, 122, 1671-1697.

NCDC, 1989: *Storm Data*, Vol. 31. [Available from National Climatic Data Center, 151 Patton Avenue, Asheville, NC 28801-5001.]

Nielsen-Gammon, J. W., and W. L. Read, 1995: Detection and interpretation of left-moving severe thunderstorms using WSR-88D: A case study. *Wea. Forecasting*, 10, 127-140.

Orville, R. E., 1991: Lightning ground flash density in the contiguous United States–1989. *Mon. Wea. Rev.*, 119, 573-577.

Reap, R. M., and D. R. MacGorman, 1989: Cloud-to-ground lightning: Climatological characteristics and relationships to model fields, radar observations, and severe local storms. *Mon. Wea. Rev.*, 117, 518-535.

Renick, J. H., 1971: Radar reflectivity profiles of individual cells in a persistent multicellular Alberta hailstorm. Preprints, *7th Conf. on Severe Local Storms*, Kansas City, MO, Amer. Meteor. Soc., 63-70.

Stolzenburg, M., 1994: Observations of high ground flash densities of positive lightning in summertime thunderstorms. *Mon. Wea. Rev.*, 112, 1740-1750.

Tuttle, J. D., V. N. Bringi, H. D. Orville, and F. J. Kopp, 1989: Multiparameter radar study of a microburst: Comparison with model results. *J. Atmos. Sci.*, 46, 601-620.

Wilson, J. W., and D. Reum, 1988: The flare echo: Reflectivity and velocity signature. *J. Atmos. Ocean. Technol.*, 5, 197-205.

Zrnic, D. S., 1987: Three-body scattering produces precipitation signature of special diagnostic value. *Radio Sci.*, 22, 76-86.